A Circuit for Detection of Interaural Time Differences in the Nucleus Laminaris of Turtles

Katie L. Willis [1,2] and Catherine E. Carr [1]

1 University of Maryland, Department of Biology, Center for Comparative and Evolutionary Biology of Hearing, Neuroscience and Cognitive Science Graduate Program
2 Present address: University of Oklahoma, Department of Biology
kwillis@ou.edu

Key words: sound localization, interaural time difference, turtle, binaural hearing

Summary Statement: Turtles share the auditory brain stem connectivity with other reptiles, including birds, and encode interaural time differences in nucleus laminaris.

List of abbreviations

ABR: Auditory brainstem response
ACSF: Artificial cerebrospinal fluid
BF: Best frequency
CD: Characteristic delay
CP: Characteristic phase
ITD: Interaural Time Difference
IPD: Interaural Phase Difference
NA: Nucleus angularis
NL: Nucleus laminaris
NM: Nucleus magnocellularis
SO: Superior olive
TS: Torus semicircularis
VS: Vector strength

Abstract

The physiological hearing range of turtles is about 50-1,000 Hz, as determined by cochlear microphonics (Wever and Vernon, 1956a). These low frequencies can constrain sound localization, particularly in Red-eared Slider Turtles, which are freshwater turtles with small heads and isolated middle ears. To determine if these turtles were sensitive to interaural time differences (ITDs), we investigated the connections and physiology of their auditory brainstem nuclei. Tract tracing experiments showed that the VIII nerve bifurcated to terminate in the first order nucleus magnocellularis and nucleus angularis, and the nucleus magnocellularis projected bilaterally to nucleus laminaris. Since the nucleus laminaris received inputs from each side, we developed an isolated head preparation to examine responses to binaural auditory stimulation. Magnocellularis and laminaris units responded to frequencies from 100-600 Hz, and phase locked reliably to the auditory stimulus. Responses from the nucleus laminaris were binaural, and sensitive to ITD. Measures of characteristic delay revealed best ITDs around ± 200μs, and nucleus laminaris neurons typically had characteristic phases close to 0, consistent with binaural excitation. Thus, turtles encode ITDs within their physiological range, and their auditory brainstem nuclei have similar connections and cell types to other reptiles.

Introduction

Tympana have evolved multiple times in lineages leading to extant amphibians, reptiles and mammals (Clack, 1997; 2002; Carr and Christensen-Dalsgaard, 2016, Willis et al., 2013a). In turtles, adaptations of the tympanum have produced an ear that is somewhat more sensitive underwater than in air, but still adapted to an amphibious lifestyle, as shown both by laser vibrometry measures of tympanum responses in air and water, and by auditory brain stem responses (ABR) in air (Christensen-Dalsgaard et al., 2012; Willis et al., 2013b). In a commonly studied model, the Red-eared Slider Turtle, *Trachemys scripta elegans*, the tympanum is a disk about 0.5 mm thick that moves via a hinged connection to the bony capsule wall surrounding it (Christensen-Dalsgaard et al., 2012; Wever and Vernon, 1956b). In air, sound pressure moves the tympanic disk. When submerged, the air in the middle ear cavity resonates in the underwater sound field, which drives the tympanic disk from within the skull (Christensen-Dalsgaard et al., 2012).

In air, Red-eared Sliders are relatively insensitive to sound, hearing low frequencies at comparatively high thresholds, mostly below 1 kHz and above 40 dB SPL (Christensen-Dalsgaard et al., 2012; review in Manley, 2010). Hair cells in their basilar papilla are tuned

to specific frequencies in the acoustic stimulus from near 20 Hz to above 500 Hz, through an electrical resonance mechanism (Art et al., 1986; Crawford and Fettiplace, 1981a, b). Despite the prominence of turtles as a model of hair cell tuning (e.g. Fettiplace and Fuchs, 1999), relatively little is known about their central auditory system (for review, see Willis et al., 2013a), with the notable exception of immunohistochemical studies of the central auditory system in pond turtles (Belekhova et al., 1985; 2002; 2008; 2010). Ethological relevance is added by recent findings that *Chelodina oblonga,* a side-necked, freshwater turtle, emits sounds underwater that may be used for communication (Giles et al., 2009). Finally, the position of testudines relative to other vertebrate taxa has been resolved. Molecular analyses have identified testudines as a sister group to the archosaurs (Chiari et al., 2012; Lu et al., 2013; Shen et al., 2011), a group characterized by sensitive hearing. This newly clarified evolutionary relationship motivated our investigation of the turtle auditory system in order to compare it with that of other reptiles.

In all reptiles, the auditory branch of cranial nerve VIII bifurcates to terminate in the first order nucleus magnocellularis and the nucleus angularis. The nucleus magnocellularis projects bilaterally to the nucleus laminaris. Nucleus laminaris and nucleus angularis then project to the midbrain torus semicircularis (for reviews, see Carr and Code, 2000; Grothe et al., 2004; Willis et al., 2013a). Previous work on turtles showed that the auditory branch of the VIII nerve projected to nucleus magnocellularis and nucleus angularis (Marbey and Browner, 1985; Sneary, 1988). Putative nucleus magnocellularis cell types have also been described in turtles (Browner and Marbey, 1988). However, a difficulty in many of the older studies lay in the identification of nucleus borders. For example, Miller and Kasahara (1979) were not able to identify a clear projection from the nucleus magnocellularis to the nucleus laminaris, or differentiate between nucleus magnocellularis and nucleus laminaris. We therefore used more recently developed techniques to define the auditory nuclei and their connections. Since turtles have been identified as a sister group to the archosaurs, we hypothesized that connections among their auditory nuclei would follow the archosaurian pattern.

It can be difficult to maintain a stable plane of anesthesia in turtles without activation of the head withdrawal reflex. In parallel with the tract tracing studies, we therefore developed an isolated head preparation to investigate the physiology of the central auditory system. Crawford and Fettiplace (1981a) had previously developed a half-head preparation for neurophysiological studies of hair cells and auditory nerve (Crawford & Fettiplace, 1981a; 1983; Art & Fettiplace, 1987; Art et al., 1995; Hailey et al. 1991). The basilar papilla of turtles can be isolated and recorded from *in vitro* (e.g. Schnee et al., 2005; 2011; 2013) and models of hair cell stereocilia have been derived from isolated turtle basilar papilla preparations

(Breneman et al., 2009). In other experiments, turtle isolated head or isolated brain regions have been used to examine properties of cerebellum (Rice and Nicholson, 1990), and cortex (Larkum et al., 2008). Turtle cortex is three-layered, and been studied in a visual cortex preparation that can include the optic nerve and eye (Connors and Kriegstein, 1986; Kriegstein and Connors, 1986; Mancilla et al., 1998; Du et al., 2006). The mitral cells of the turtle olfactory bulb have been studied *in vitro* (Mori et al., 1981). Cortical experiments have used chronically implanted electrodes *in vivo* (Rutishauser et al., 2013) as well as *in vitro* (Du et al., 2006; Rice and Nicholson, 1990).

In the whole head preparation, we used a craniotomy to expose the areas of interest, and dichotic stimulation to test response properties of neurons. In accordance with auditory brain stem response (ABR) measurements (Christensen-Dalsgaard et al., 2012), and cochlear potentials (Wever and Vernon, 1956a,c), we hypothesized that the turtle brain stem would be most responsive to frequencies under 1 kHz and encode a small range of ITDs, consistent with its head size.

Methods

All experiments were carried out with the approval and under the guidelines of the University of Maryland Institutional Animal Care and Use Committee, and in accordance with the National Institutes of Health Guide for the Care and Use of Laboratory Animals.

Surgery and Anesthesia

Adult Red-eared Slider Turtles (*Trachemys scripta elegans*) of both sexes were obtained from Kon's Direct (Germantown, WI). Animals ranged from 10-15 cm in carapace length; 10 cm carapace is the minimum size turtle allowed to be sold (Title 21 CFR 1240.62, United States Code of Federal Regulations). Animals were group housed and maintained on a 12 h light/ 12 h dark cycle. For anesthesia before all procedures, Propofol (5mg/kg; MacLean et al., 2008) was administered intravenously through the subcarapacial vein, which lies immediately below where the neck meets the carapace. After cessation of all reflexes, animals were rapidly decapitated. The brain was exposed to allow for sufficient volume of flow (~1mL/min) of oxygenated artificial cerebrospinal fluid (ACSF) composed of 96.5mM NaCl, 2.6mM KCl, 4.4mM $CaCl_2$, 2.0mM $MgCl_2$, 31.5mM $NaCO_3$, and 10mM dextrose dissolved in distilled water (Connors and Kriegstein, 1986).

Tract Tracing and Golgi

Neurobiotin (Life Technologies, Grand Island, NY) was applied to brain stem or midbrain structures, using either iontophoresis of 4% Neurobiotin in 0.9% saline (1-2μA alternating positive current for 10 minutes) or application of neurobiotin on the tip of a tungsten microelectrode (see below). For dye transport, tissue was immersed in a 4°C incubator, with oxygen-saturated ACSF changed every 24 hours. Transport time varied from 1-96 hours; anterograde transport from nucleus magnocellularis to the ipsilateral nucleus laminaris was brief (12 hours) while retrograde transport from torus semicircularis to the nucleus angularis or the nucleus laminaris took longer (2 days). The tissue (midbrain, hind brain) was immersion fixed in 4% paraformaldehyde in 0.01M phosphate buffered saline (PBS) for 18-24 hours. The brain was then cryoprotected in 30% sucrose in 0.01 M PBS. Tissue was cut on a freezing microtome in 80 μm sections and rinsed in 0.01 M PBS. Sections were incubated in avidin biotin complex (ABC kit, Vector Labs, Burlingame, CA), in 0.2% Triton in 0.01M PBS solution for 1-4 hours at room temperature, and then reacted using the Vector SG Peroxidase (HRP) Substrate Kit, Vector Labs) for 10-20' then rinsed with 0.01M PBS. Tissue was counterstained with neutral red or cresyl violet, dehydrated and cleared. Labeled neurons were digitally reconstructed using NeuroLucida (MBF Bioscience, Williston, VT). Measurements were made using NeuroExplorer (MBF Bioscience, Williston, VT).

The rapid Golgi technique was used on five young turtles (carapace 2.5 cm length) (Valverde, 1970). Brains were removed and placed in Golgi fixative, an aqueous solution containing 2.33% potassium dichromate and 0.19% osmium tetroxide. After one week, the brains were rinsed in 0.75% aqueous silver nitrate, and stored for 24 hours in a fresh volume of 0.75 % silver nitrate. Brains were then sectioned at 100μm. Magnocellular and laminaris neurons were found in 4 brains.

Electrophysiology

The isolated turtle brain preparation offers advantages over traditional *in vivo* and *in vitro* (slice) preparations. Keeping the ear intact enables use of acoustic instead of electrical stimuli, and an isolated head preparation avoids the difficulties of keeping a turtle sufficiently anesthetized. Maintaining a turtle at the appropriate plane of anesthesia is difficult because the head withdrawal response may return even with a surgical plane of anesthesia. This preparation also provides unrestricted access to the dorsal brain stem, normally obscured by a large sinus.

We maintained the preparation at 24-30°C (Table S1), in order to match the temperature at which the animals are housed.

The most effective ACSF was developed by Connors and Kriegstein (1986; Table S1). These preparations remained responsive for 4-14 hours; one preparation was responsive after being immersed in oxygenated ACSF in a 4°C refrigerator overnight. ACSF was bubbled with 95% O_2-5%CO_2 gas for 10 minutes before initial use and again every 2-3 hours. We used an ACSF drip through IV tubing to superfuse the brain. The head was held in a constant position by a stainless steel head post glued to the prefrontal bone. Recordings were made with 125 µm tungsten microelectrodes (F. Haer, Bowdoin ME), with impedances around 20 MΩ. Electrodes were positioned above the acoustic tubercle, a prominence of the floor of the lateral recess of the fourth ventricle that contains the primary and secondary auditory nuclei (Fig. 1). Electrodes were advanced remotely in 5-10 µm steps, while continuously testing for auditory responses. Responses were amplified (µA200, Walsh electronics), high-pass filtered at 300 Hz, and passed to an A/D converter (TDT DD1). Both the analog and the TTL signals were stored and processed by custom-written software ("Xdphys" written in Dr. M. Konishi's laboratory at California Institute of Technology, CA). Recordings were made in a sound-attenuating chamber (IAC, Hanover MD). Closed, custom-made sound systems were placed around the tympanic disk on both ears, containing commercial miniature earphones and miniature microphones (Knowles EM 3068). These were sealed against the head using Gold Velvet II ear impression material (All American Mold Laboratories, Oklahoma City, OK). The sound systems were calibrated individually before the recordings.

Acoustic stimuli were digitally generated by Xdphys, driving a signal-processing system (Tucker Davis Technology, Gainesville, FL). Stimuli were generated separately for the two ears by using a TDT AP2 signal processing board. Both channels were then fed to the earphones via D/A converters (TDT DD1), anti-aliasing filters (TDT FT6-2), and attenuators (TDT PA4). Tone bursts had 100ms duration (including 5ms linear ramps) and were presented at a rate of 5/s and thus a duty cycle of 50%. We measured monaural iso-level frequency responses and rate-intensity functions at best frequency. Interaural time differences (ITD) were tested within ± 1 stimulus period, in steps no larger than 1/10 of the period and stimulus durations of 100 ms. Stimulus levels were between 70-85 dB SPL, and 10-15 stimulus repetitions were presented at each ITD.

Only single units were used for ITD analysis (characteristic delay, mean phase). Single units were isolated as distinct spikes above the recording baseline, with the presence of a refractory period in the interspike-interval histogram. To calculate characteristic delays (CD), we fitted spike rate as a function of ITD with a cosine function at the respective stimulus frequency to determine best interaural phase difference, or the peak

closest to zero interaural phase difference (Viete et al. 1997, Matlab, Natick MA). After measuring tonal ITD curves at many frequencies within the frequency-response-area of a cell, we plotted the mean interaural phase, which represents the peak of the periodic ITD curve in cycles, as a function of frequency. In these plots, the slope of the linear regression is the CD, and the y-intercept the characteristic phase (CP; Yin and Kuwada 1983). CPs were between 0.25 and -0.25 cycles.

Results

Hindbrain auditory nuclei

On each side, the hindbrain contained four auditory nuclei (Fig. 1; Belekhova et al., 1985, Miller and Kasahara, 1979). The first order nuclei, the nucleus angularis and the nucleus magnocellularis, were located dorsal and medial in the acoustic tubercle. A second order nucleus, the nucleus laminaris, was also located in the acoustic tubercle, below the nucleus magnocellularis. Nucleus magnocellularis, nucleus laminaris, nucleus angularis, the superior olive (SO), and the torus semicircularis (TS; in the midbrain) were found in similar locations to lizards and birds (reviews in Carr and Code, 2000; Willis et al., 2013a).

All nuclei formed rostro-caudal columns. In Nissl stained material, the borders of the auditory nuclei could be distinguished in both cresyl violet (Fig. 2A) and neutral red stained material (Fig. 2B, 3B, C). From caudal to rostral, the nucleus magnocellularis was most caudal, and the rostral portion of nucleus magnocellularis overlapped the caudal portion of nucleus laminaris. Next, nucleus laminaris was ventral to nucleus magnocellularis and nucleus angularis (Fig. 1). The caudal part of nucleus angularis overlapped the rostral part of nucleus laminaris and lay dorsal to nucleus laminaris. Both the nucleus angularis and nucleus magnocellularis were superficial, located on the medial edge of the brainstem below the IV ventricle (Fig. 1). Nucleus angularis was also superficial and medial, caudal to the cerebellar peduncle. In transverse sections, nucleus magnocellularis was round, while nucleus angularis had a roughly ovoid shape, but became more round rostrally. Caudally, nucleus angularis had less defined borders, forming a polygonal outline in reconstructions. Nucleus laminaris formed a crescent in transverse section. It was more compact medially and spread out in the dorso-ventral axis more laterally. The superior olive was a round nucleus in the ventral brain stem, below nucleus laminaris (see Fig. 4B).

In addition to position, nuclei were defined by their afferent and efferent connections. Tract tracing experiments revealed the connections of the brainstem nuclei. The nucleus angularis and the nucleus magnocellularis received input from the ipsilateral VIII nerve. The details of these projections are the subject of another study (Willis, et al., 2014). Nucleus

magnocellularis projected bilaterally to nucleus laminaris, and contralaterally projecting nucleus magnocellularis axons formed a distinctive cross-tract, termed the acoustic stria, above the medial longitudinal fasciculus (Fig. 2D, see Fig. 4 for a summary). After crossing the midline, nucleus magnocellularis axons ascended into the contralateral acoustic tubercle and arborized in the neuropil below the contralateral nucleus laminaris cell body layer. Neurobiotin injections into nucleus magnocellularis consistently yielded axons in the acoustic stria and terminals below the nucleus laminaris (n=6), while neurobiotin injections into the nucleus laminaris retrogradely labeled neurons in the contralateral nucleus magnocellularis (53 neurons, n = 4 cases, Fig. 2B, C). Retrogradely labeled nucleus magnocellularis neurons were distributed approximately equally among the 4 cases.

Reconstruction of retrogradely and Golgi labeled magnocellular neurons revealed cell body areas of about 150 μm (139.9 ± 68.3, n = 70), and a varied number of dendrites (Fig. 2B, C; 4A). Some magnocellularis neurons appeared to have short or no dendrites, while others had dorsally directed dendritic arbors that penetrated the VIII nerve tract above nucleus magnocellularis (Fig. 2C). Despite these differences in dendritic arbors, nucleus magnocellularis appeared to contain a single cell type on the basis of cell body size and form factor. Nucleus magnocellularis cell bodies tended to be rounder (form factor= 0.85 ± 0.07) and smaller than nucleus angularis somata. Using ANOVA, three main features separated the primary and secondary auditory nuclei. Nucleus angularis soma areas were larger than nucleus laminaris or nucleus magnocellularis ($p < 0.01$,$f = 18.81$, n= 189). Nucleus angularis soma form factors were smaller than nucleus magnocellularis and nucleus laminaris (i.e. nucleus magnocellularis and nucleus laminaris soma were more round, $p < 0.05$, $f = 2.32$, n = 189). Finally, nucleus laminaris average dendrite length was greater than nucleus magnocellularis and nucleus angularis ($p < 0.01$, $f = 21.25$, n = 189). Both retrogradely labeled neurobiotin filled neurons and reconstructed Golgi stained neurons were included in this analysis, which is reflected in the n values.

In addition to receiving bilateral projections from the nucleus magnocellularis, the nucleus laminaris was identified by its rostrocaudal position between the nucleus magnocellularis and the nucleus angularis, by the lack of auditory nerve inputs, and by retrograde labeling of its neurons after dye injections confined to the torus semicircularis. Nucleus laminaris neurons formed a lamina that was compact medially and spread laterally (Fig. 3, 4A). This lamina was characterized by bitufted neurons (retrogradely labeled and reconstructed, n = 45). The nucleus laminaris soma had an average form factor of 0.86 ± 0.1 and an average area of 143.5 ± 56.3 μm (n = 45). In medial nucleus laminaris, the dendrites of the bitufted neurons were dorso-ventrally oriented (Fig. 3, 4A). More laterally, the nucleus laminaris lamina became less compact, neurons tended to spread apart, and their orientation became less strictly dorso-ventral (Fig. 3E, arrow). The lateral edge of the

nucleus laminaris tended to curve ventrally, and some neurons were separated from the main lamina of the nucleus (Fig. 3C, E). Within the main lamina of nucleus laminaris, the dendrites were bitufted, with dorsal dendrites extending into the nucleus magnocellularis or dorsal fiber bundles, and ventral dendrites arborizing below laminaris. Measures of dendritic orientation with respect to the lamina of nucleus laminaris cell bodies showed a largely orthogonal orientation (Fig. 3E insert, grey lines), while dendritic orientations in the lateral, curved region of the nucleus laminaris were less strictly oriented (Fig. 3E insert, black lines). Nucleus laminaris neurons projected bilaterally to torus semicircularis, as seen from retrograde labeling using neurobiotin (NB; 4 cases) and horseradish peroxidase injections into the torus semicircularis (HRP; 2 cases) (Fig. 3, 4B).

Dye injection into the torus semicircularis also labeled ascending lemniscal fibers from the ipsilateral nucleus angularis and ipsilateral superior olivary nuclei (n= 6 cases). The nucleus angularis and the superior olive projected to the lemniscal nuclei and to the torus semicircularis, which forms the dorsal portion of caudal midbrain, just rostral to the cerebellar peduncles and caudal to the optic tectum. Nucleus angularis projected bilaterally to torus semicircularis, with the contralateral projection being more prominent than the ipsilateral one. Thus, the brain stem auditory nuclei followed the connectivity pattern previously shown for the pond turtles *Emys orbicularis* and *Testudo horsfieldi* (Belekova 1985) and for all other reptiles, including birds (Fig. 4B).

Isolated Head Preparation

In turtles, the ACSF formulation and temperature control were key to obtaining viable recordings (Table S1). The recipe we used was optimized for turtle *in vitro* recordings. The superfusion rates of oxygenated ACSF were similar to the setup of other *in vitro* physiology experiments. Keeping the preparation warm (25-30°C) by using a commercial space heater to heat the sound-attenuating chamber yielded the largest number of stable recordings. The temperature at which we obtained stable recordings overlapped with the temperature range at which the animals were housed (25-30°C). We began by using the ACSF recipe used in avian slice preparations (e.g. MacLeod and Carr, 2005). Tissue maintained in avian ACSF was healthy enough for dye transport but not for physiological recordings. Another ACSF solution used for one experiment contained 0.005 M imidazole; the preparation was only viable for about 1 hour (two units recorded) with this ACSF (Table S1, Rodgers-Garlick et al., 2013). We also used a solution developed for an *in vitro* turtle cerebellum preparation that contained tetramethylammonium chloride (Rice and Nicholson, 1990), which also yielded viable preparations for about 1 hour. We ultimately obtained the best results with regularly

oxygenating the solution used by Connors and Kriegstein (1986), and with a perfusion rate of about 1mL/min over the surface of the medulla.

Physiological characteristics of nucleus magnocellularis

In the isolated brain preparation, the acoustic tubercle appeared as a well-delineated expansion of the medial wall of the medulla. Recordings from the isolated brain preparation provided data on responses to auditory stimulation in nucleus magnocellularis. We report the frequency tuning, phase-locking and responses to increasing sound intensity of 123 nucleus magnocellularis units from 29 animals, recorded from the dorsal portion of the acoustic tubercle, with depths from the brain surface ranging from 107±82 µm, n=101. Nucleus magnocellularis units only responded to ipsilateral sound and could therefore be differentiated from nucleus laminaris responses. Sound pressure levels (SPL) used were typically within 10 to 20 dB above threshold at each frequency. Best frequencies in nucleus magnocellularis ranged from 100-600 Hz (Fig. 5). Auditory thresholds measured at best frequency revealed mean thresholds of 69.2 ± 9.12 dB SPL (n = 123, Fig. 5B,C). The lowest recorded single unit thresholds were 40 dB SPL, for three units, with best frequencies of 150, 220 and 400 Hz, respectively. Average physiological thresholds were high, compared to other reptiles and also above thresholds recorded *in vivo* from the common box turtle (mean of 48 dB SPL, ±8, n=24, measured from Figure 1 of Manley, 1970). Thresholds were generally similar to, but below, the thresholds derived from ABR audiograms (Fig. 5, Christensen-Dalsgaard et al., 2012).

Nucleus magnocellularis units reliably phase locked to the stimulus (Fig. 6, sample phase histogram in 6A insert). Phase-locking is measured using a period histogram (Fig. 6A, insert), which plots the instantaneous firing rate as a function of stimulus phase in cycles. The degree of phase-locking is typically quantified using the metric of vector strength (Goldberg and Brown, 1969, Ashida and Carr, 2010). Vector strength falls between 1 (all spikes in a single bin) and 0 (no phase-locking). In the turtle recordings, phase locking was measured at best frequency. We observed almost no changes in vector strength with frequency (Fig. 6A). In nucleus magnocellularis, phase locking vector strength varied from 0.53-0.97, averaging 0.82 ± 0.07 (n = 123). Firing patterns tended to be primary-like (Fig. 6B), characterized by a phasic peak of activity at the beginning of the stimulation, followed by a tonic discharge at a lower rate for the rest of the stimulus period. We also recorded units with more sustained responses to stimulation (Fig. 6C, D).

Figure 6C and D shows responses from a magnocellularis neuron, with a best frequency of 180 Hz, to a 100 ms tone. The dot raster (panel C) indicates the occurrence of spikes, relative to the stimulus, upon 50 repeated presentations of the same tone (see Joris et al., 2006). The vertical patterning of the dots show that spikes occur at a preferred phase of the stimulus. This is more easily seen in the post stimulus time histogram (panel D) in which the spikes from this neuron are aligned with the onset, or a fixed phase point, of an identical stimulus presented 100 times. The aligned sequences are superimposed in time, and then used to construct a histogram. Measurements of the interspike intervals (Fig. 6D, insert) show the expected stimulus period of 5.55ms associated with stimulation at 180Hz.

Physiological characteristics of nucleus laminaris

We recorded from nucleus laminaris units in the dorsal portion of the acoustic tubercle in 13 different animals, both below nucleus magnocellularis and sometimes more rostral than nucleus magnocellularis (mean depths of 210±73 µm, n=45). Physiologically, nucleus laminaris units were defined by responses to stimulation of both the ipsilateral and contralateral ears, and were sensitive to interaural time differences (ITD). While we obtained both single (n = 45) and multi-unit (n = 20) recordings in nucleus laminaris, we did not include multi-units in our measurements of ITD. In order to determine the frequency-independent ITD, we measured ITDs in a range of different frequencies within the frequency-response-area of a cell, and plotted the mean interaural phase, which represents the peak of the periodic ITD curve in cycles, as a function of frequency. In these plots, the slope of the linear regression is the CD, or characteristic delay, while the y-intercept is the characteristic phase (CP). Not all 45 nucleus laminaris recordings included all measurements. We have 21 complete data sets with ipsi-, contra- and binaural measurements of best frequency, threshold, vector strength, ITD sensitivity, and characteristic delay.

We report the frequency tuning, phase locking, and responses to increasing sound intensity of nucleus laminaris units. Auditory thresholds measured at best frequency were generally similar to thresholds in nucleus magnocellularis, and typically below the thresholds derived from ABR audiograms (Fig. 7A). Units had a mean threshold of 71.2 ± 8.27 dB SPL (n = 40; Fig. 7A). The lowest single unit threshold was 55 dB SPL. In nucleus laminaris, recorded best frequencies ranged from 100-700 Hz (Fig. 7). In general, nucleus laminaris units responded similarly to stimulation of either ear. In six cases, however, the nucleus laminaris units had lower thresholds and stronger responses to ipsilateral broadband noise than to a particular frequency. All contralateral inputs to nucleus laminaris units were tuned

to a particular frequency, and in these cases, the contralateral BF was used to drive the neuron for measures of phase locking, sensitivity to changes in level, and responses to changing ITD.

Neurons in the nucleus laminaris were sensitive to ITD over a range of frequencies around their best frequency (Fig. 8). Nucleus laminaris units reliably phase locked to both ipsilateral and contralateral stimuli (Fig. 8D). We measured phase locking at best frequency, and at 20 dB SPL above threshold, and found almost no changes in vector strength with frequency (Fig. 7B). In nucleus laminaris, phase locking vector strength from single units varied from 0.22-0.97, averaging 0.79 ± 0.06 (n = 45) (Fig. 7B; sample phase histograms in Figure 8D). Nucleus laminaris firing patterns tended to be sustained (Fig. 7C, D, 8B). We used monaural phase locked responses to compute peak phase differences between ipsi- and contralateral period histograms. These phase differences reflected each nucleus laminaris neuron's best ITD (Fig. 8F). Nucleus laminaris neurons were excited by both ears; i.e. they were "peak type" neurons, with measures of characteristic phase (CP) typically close to 1 or 0, with the CP defined as the phase intercept at 0 Hz in plots of mean interaural phase versus stimulus frequency of the response (Kuwada et al. 1987; Yin and Kuwada 1983, Fig. 8E insert). Peak-type neurons displayed ITD functions where the peaks (maxima) were aligned at a particular ITD across frequency (CPs between 0.0 and ±0.25 cycles). CPs averaged -0.025 ± 0.038, n = 21, Fig. 8D insert). We calculated fewer CDs than best ITDs because we did not have a sufficient range of frequencies (minimum of five different frequencies for CD calculation) for characteristic delay for all recordings.

We performed a detailed analysis of the sensitivity to ITDs in the fine structure of low-frequency pure tones in the subset of 21 nucleus laminaris neurons for which we were able to obtain a complete set of recordings (Fig. 9). Our measures of characteristic delay showed that turtles were sensitive to ITDs from -200 to 200 μs, with best ITDs centered around 0μs (mean -9μs ± 68, n = 21, where positive ITDs represent the ipsilateral ear) (Fig. 9). These peaks were generally within or close to the physical range of ITDs available to Red-eared sliders, which have fairly small heads and ears that are not coupled (Willis et al., 2013b). For estimates of the physical range available to Red-eared slider turtles, we used the range of ITDs possible for a large animal (12 inch or 30.5 cm carapace, about 6 cm head width), and the speed of sound in air. We note, however, that we recorded from medium sized turtles, with a maximum head width of 32 mm. The distribution of recorded ITDs showed a slight asymmetry towards negative values, i.e. to sound originating from the contralateral hemisphere (Fig. 9B, C).

Discussion

We developed an isolated head preparation to analyze neural circuits in the auditory brainstem of the Red-eared slider turtle. Recordings from the first order nucleus magnocellularis and its target, the nucleus laminaris, revealed neurons sensitive to best frequencies between 100-600 Hz, that phase locked to the auditory stimulus. Best ITDs recorded in the nucleus laminaris were consistent with the turtle's physiological range, or range of time differences determined from their interaural distance.

ITDs conformed to the range of time differences predicted by head size

This is the first demonstration of neural sensitivity to ITDs in turtles, and suggests that they may be able to localize sound sources, albeit poorly. Our data suggest that the largely homogeneous and broadly-tuned ITD-sensitive population of neurons in turtle laminaris could encode spatial position by changes in spike rate across the span of physiological ITDs. Turtle neurons have low best frequencies, with the lowest best frequency neurons having, necessarily, the broadest ITD functions in response to interaurally delayed signals. Thus, even for relatively large changes in ITD, encompassing perhaps the entire range experienced by an animal like the Red-eared Slider Turtle, the response near the peak of the function may change only slightly (Fig. 9A).

Two strategies have emerged to improve localization when low frequency hearing and small heads limit animal's' ability to encode sound source location. Other reptiles, like lizards and archosaurs, have coupled ears, which increase the range of ITDs available at low frequencies (Calford and Piddington, 1988; Christensen-Dalsgaard and Manley, 2008; Carr and Christensen-Dalsgaard, 2016; Carr et al., 2016; von Hemmen et al., 2016; Larsen et al., 2016). Small mammals, such as the gerbil and guinea pig, show a trend that places the sensitive slope of the function where greatest ITD discrimination is required (McAlpine et al., 2001, for reviews see Grothe et al, 2010; Grothe and Pecka, 2014). By shifting the peak ITD closer to zero for neurons as characteristic frequency increases, the position of the slope through the range of relevant ITDs is maintained. Neither strategy applies to the data presented here, since turtle ears are not coupled and our recordings show ITD peaks largely within their physiological range in air (Fig. 9C).

The combination of small head size, low frequency hearing and uncoupled ears should make it difficult for the turtle nucleus laminaris to encode a range of ITDs in air. The wavelength of sounds below 1 kHz is much greater than the turtle head size, with wavelengths of 100 Hz in water being about 3.4 m, and about 70 cm in air. Turtle ears are not acoustically coupled, and their middle ears are connected to the pharynx by thin

Eustachian tubes (Willis et al., 2013). Middle ears that are not coupled may be an adaptation for hearing underwater (Christensen-Dalsgaard et al., 2012, Willis et al., 2013). Turtle ITD sensitivity may, however, allow these animals to navigate towards or away from sound sources.

In addition to sound source localization, at least some turtles emit sounds, possibly for communication. *Chelonidina oblonga* emits sound under water, with both percussive and complex calls (Giles et al., 2009). There are also studies suggesting that hatchlings of multiple species vocalize (Ferrara et al., 2013; 2014a, b; 2017). Multiple species of tortoise vocalize during mating (e.g. Campbell and Evans, 1967). Although there are no audiograms (behavioral or derived from physiological tests, like ABR) for most of these species, published audiograms for testudines show a hearing range below 1 kHz with lowest thresholds around 300-600 Hz.

Although the increased speed of sound in water should further reduce the turtle's range of ITDs, most best ITDs in air were close to 0 µs, so if both ears are driven together underwater, best ITDs should remain clustered near 0 µs. It is unlikely that turtles could use the underwater localization cues available to bony fishes, where sound source localization depends upon arrays of hair cells with different orientations (for review, see Edds-Walton, 2016). Scanning electron microscopic studies showed that the hair cells of turtle papillae are unidirectional (Miller, 1978). Miller describes the papillae of turtles as relatively large and characterized by a long, horizontal middle section resting on a wide basilar membrane (Miller, 1978).

Organization of turtle brainstem circuits consistent with phylogeny

Understanding of testudines' low frequency hearing may be complicated by their adaptation to hearing underwater (Christensen-Dalsgaard et al., 2012; Willis et al., 2013b). Since sound travels much faster in water than in air, hearing underwater might have effects on neural processing that may not be revealed by anatomical experiments, or by physiological studies in air. Nevertheless, the neural circuits described here share similar connections and cell types to other reptiles, including birds. The auditory nerve bifurcates to terminate in the nucleus magnocellularis and the nucleus angularis, while the nucleus magnocellularis projects bilaterally to the nucleus laminaris. Nucleus laminaris and nucleus angularis then project to the midbrain torus semicircularis (for reviews, see Carr and Code, 2000; Grothe et al., 2004; Willis et al., 2013a).

In birds, lizards and mammals, which have a wider range of hearing frequencies than turtles, the brain stem nuclei appear proportionally larger in size. For example, in birds and lizards, the nucleus angularis is more differentiated than in turtles, with several neuron types

(for review, see Grothe et al., 2004; Soares and Carr, 2001, Szpir et al., 1995). In our material, measurements of neuron size, number and orientation of dendrites, and form factor of reconstructed neurons did not reveal different cell types within either the nucleus magnocellularis or angularis. One option for differentiating neurons further would be to use immunohistochemical techniques, expanding on the work of Belekhova et al. (2002), who examined calcium binding protein expression in turtle auditory structures. Belekhova and coworkers found parvalbumin, calbindin, and calretinin immunoreactivity in nucleus magnocellularis, nucleus angularis, and nucleus laminaris (Belekhova et al., 2008) and in torus semicircularis (Belekhova et al., 2010).

Multiple theories have been put forward to explain the emergence of diverse neuronal structure-function relationships. One explanation is that specific cell types differentiate to process specific parallel streams of information. Increases in high-frequency sensitivity in lepidosaurs (Manley, 2002) and in other archosaurs, such as birds and crocodilians, may have increased selection for neurons to differentiate in the nucleus angularis in order to process parallel streams of information. In order to support or refute this hypothesis, recordings from turtle nucleus angularis are necessary. If the addition of higher frequency hearing drives differentiation into multiple cell types, turtles might more closely resemble the archosaur ancestral condition, since there is no evidence that the common ancestors of archosaurs were auditory specialists. It is more likely that early archosaurs were sensitive to low frequency sound (Gleich et al., 2004), as is the case for turtles.

Best frequencies and thresholds in the isolated head preparation

Isolated neural preparations have been developed in a variety of animals, including many invertebrates. Some of these leave relevant peripheral structures intact. In mammals, isolated brain preparations are generally maintained by perfusion through the basilar artery with a blood substitute or ACSF (Llinás and Mühlethaler, 1988). In other cases, the isolated tissue is typically submerged in ACSF or saline. The time over which this preparation remains viable depends largely on the species.

The range of best frequencies recorded in the isolated turtle brain preparation was consistent with published ABR audiograms (Christensen-Dalsgaard et al., 2012), suggesting that the isolated preparation was viable. We recorded responses from 100 to 800 Hz; the highest single unit best frequency recorded in nucleus magnocellularis was 454 Hz, and the highest best frequency multiunit response was 620 Hz. In nucleus laminaris, the highest best frequency single unit recorded was 600 Hz. These values were similar to recordings from the auditory brain stem of an intact anesthetized *Terrapene carolina* (Common Box Turtle; Manley, 1970), where 500 Hz was the highest characteristic frequency (Fig. 5C). Thus, *in*

vivo recordings yielded similar best frequency responses to those from our isolated brain preparations.

Similar best frequency ranges of 100-400 Hz were recorded in prior isolated brain experiments in turtles (Hailey et al., 1991). Although it was possible that higher temperatures might yield higher best frequencies, Hailey et al. (1991) used temperatures up to 40 °C and found no units with a best frequency above 400 Hz. Similar results were obtained from an isolated half head preparation, where Crawford and Fettiplace (1980) recorded auditory nerve units with best frequencies of 50-700 Hz, and minimum thresholds of 35 dB SPL. In the half head preparation, both hair cells and auditory nerve fibers yielded sharp tuning curves up to 600 Hz (Crawford and Fettiplace, 1980; Wu and Fettiplace, 1996). To both acoustical and mechanical displacement of hair cells, the auditory nerve responded best below 500 Hz, but could respond to high intensity stimulation (90-100 dB SPL) up 1 kHz (Crawford and Fettiplace, 1983).

Manley's 1970 *in vivo* recordings yielded similar but more sensitive responses to those from our isolated brain preparation. The lowest thresholds recorded from the cochlear nucleus of an intact anesthetized *Terrapene carolina* (Manley, 1970) were about 35 dB (mean *in vivo* thresholds computed from Manley (1970) Fig. 1 = 48±8dB, n=23; Fig. 5C). These values were comparable to the best sensitivities in *Trachemys* auditory nerve of just under 40 dB SPL (Art and Fettiplace, 1986), and comparable only to our best sensitivities of 40 dB SPL, suggesting that the *in vivo* preparation was more sensitive than the isolated brain preparation. Mean sensitivities from *Trachemys* NM were almost 20 dB higher than values recorded in vivo from *Terrapene* (69.2 ± 9.12 vs. 48±8dB SPL). The lowest recorded single unit thresholds from the isolated brain preparation were 40 dB SPL, for three units, with best frequencies of 150, 220 and 400 Hz, respectively

In all turtle studies, the lowest thresholds occurred at frequencies from 150-500 Hz. Compared to other reptiles (including birds), turtles had high thresholds and low best frequencies.

Acknowledgements

We gratefully acknowledge Catherine McCormick for expert advice and for generously providing her anatomical material, Angeline Johny for assistance with histology, and Christina O'Brien for histology and physiology assistance. We also thank Ellengene Peterson for the loan of her anatomical material, and Jose Peña for the Matlab scripts used for analysis of characteristic delay. We are gratefully for the comments of the reviewers, which have greatly improved this paper.

Funding

Supported by NIH DC00436 to CEC, and by NIH DC0466 to the University of Maryland Center for the Evolutionary Biology of Hearing.

Competing interests

The authors declare that they have no competing interests.

References

Art, J. J., Crawford, A. C. and Fettiplace, R. (1986). Electrical resonance and membrane currents in turtle cochlear hair cells. *Hear Res* **22**, 31–36.

Ashida, G., & Carr, C. E. (2010). Effect of sampling frequency on the measurement of phase-locked action potentials. **Front Neurosci**, *4*.

Belekhova, M. G., Chudinova, T. V., Kenigfest, N. B. and Krasnoshchekova, E. I. (2008). Distribution of metabolic activity (cytochrome oxidase) and immunoreactivity to calcium-binding proteins in the turtle brainstem auditory nuclei. *J Evol Biochem Phys* **44**, 354–364.

Belekhova, M. G., Chudinova, T. V., Repérant, J., Ward, R., Jay, B., Vesselkin, N. P. and Kenigfest, N. B. (2010). Core-and-belt organisation of the mesencephalic and forebrain auditory centres in turtles: Expression of calcium-binding proteins and metabolic activity. *Brain Res* **1345**, 84–102.

Belekhova, M. G., Kenigfest-Rio, N. B., Vesslkin, N. P., Rio, J.-P., Reperant, J. and Ward, R. (2002). Evolutionary significance of different neurochemical organisation of the internal and external regions of auditory centres in the reptilian brain: an immunocytochemical and reduced NADPH-diaphorase histochemical study in turtles. *Brain Res* **925**, 100–106.

Belekhova, M. G., Zharskaja, V. D., Khachunts, A. S., Gaidanenko, G. V. and Tumanova, N. L. (1985). Connections of the mesencephalic, thalamic and telencephalic auditory centers in turtles: Some structural bases for audiosomatic interrelations. *J Hirnforschung* **26**, 127–152.

Breneman, K. D., Highstein, S. M., Boyle, R. D. and Rabbitt, R. D. (2009). The passive cable properties of hair cell stereocilia and their contribution to somatic capacitance measurements. *Biophys J* **96**, 1–8.

Browner, R. H., Marbey, D. (1988) The nucleus magnocellularis in the red-eared turtle, *Chrysemys scripta elegans*: Eighth nerve endings and neuronal types. Hear Res **33**, 257-271.

Calford, M., & Piddington, R. (1988). Avian interaural canal enhances interaural delay. *J Comp Physiol A* ***162***, 503–510.

Campbell, H. W. and Evans, W. E. (1967). Sound production in two species of tortoises. *Herpetologica* **23**, 204–209.

Carr, C. E. and Christensen-Dalsgaard, J. (2016). Evolutionary trends in directional hearing. *Curr Opin Neurobiol* **40**, 111–117.

Carr, C. E. and Code, R. A. (2000). Central auditory system of birds and reptiles. In *Comparative Hearing: Birds and Reptiles.* (eds. Popper, A. N., Fay, R. R., and Dooling, R. J.), pp 197-248. Springer New York.

Carr, C. E., Christensen-Dalsgaard, J. and Bierman, H. (2016). Coupled ears in lizards and crocodilians. *Biol Cybern* **110**, 291–302.

Chiari, Y., Cahais, V., Galtier, N. and Delsuc, F. (2012). Phylogenomic analyses support the position of turtles as the sister group of birds and crocodiles (Archosauria). *BMC Biol* **10**, 65.

Christensen-Dalsgaard, J. and Manley, G. A. (2008). Acoustical coupling of lizard eardrums. *JARO* **9**, 407–416.

Christensen-Dalsgaard, J., Brandt, C., Willis, K. L., Christensen, C. B., Ketten, D., Edds-Walton, P., Fay, R. R., Madsen, P. T. and Carr, C. E. (2012). Specialization for underwater hearing by the tympanic middle ear of the turtle, *Trachemys scripta elegans*. *Proc R Soc B* **279**, 2816–2824.

Clack, J. A. (1997). The evolution of tetrapod ears and the fossil record. *Brain Behav Evol* **50**, 198–212.

Clack, J. A. (2002). Patterns and processes in the early evolution of the tetrapod ear. *J. Neurobiol* **53**, 251–264.

Connors, B. W. and Kriegstein, A. R. (1986). Cellular physiology of the turtle visual cortex: distinctive properties of pyramidal and stellate neurons. *J Neurosci* **6**, 164–177.

Crawford, A. C. and Fettiplace, R. (1980). The frequency selectivity of auditory nerve fibres and hair cells in the cochlea of the turtle. *J Physiol* **306**, 79–125.

Crawford, A. C. and Fettiplace, R. (1981a). Non-linearities in the responses of turtle hair cells. *J Physiol* **315**, 317–338.

Crawford, A. C. and Fettiplace, R. (1981b). An electrical tuning mechanism in turtle cochlear hair cells. *J Physiol* **312**, 377–412.

Crawford, A. C. and Fettiplace, R. (1983). Auditory nerve responses to imposed displacements of the turtle basilar membrane. *Hear Res* **12**, 199–208.

Du, X., Ghosh, B. K. and Ulinski, P. (2006). Encoding of motion targets by waves in turtle visual cortex. *IEEE Trans Biomed Eng* **53**, 1688–1695.

Edds-Walton, P. L. (2016). What the toadfish ear tells the toadfish brain about sound. In *Fish Hearing and Bioacoustics*, pp. 197–226. Springer.

Ferrara, C. R., Mortimer, J. A. and Vogt, R. C. (2014a). First evidence that hatchlings of *Chelonia mydas* emit sounds. *Copeia*. **2,** 245-247

Ferrara, C. R., Vogt, R. C. and Harfush, M. R. (2014b). First evidence of leatherback turtle (*Dermochelys coriacea*) embryos and hatchlings emitting sounds. *Chelonian Conserv Biol* **13**, 110–114

Ferrara, C. R., Vogt, R. C. and Sousa-Lima, R. S. (2013). Turtle vocalizations as the first evidence of posthatching parental care in chelonians. *J Comp Psychol* **127**, 24–32.

Ferrara, C. R., Vogt, R. C., Eisemberg, C. C. and Doody, J. S. (2017). First evidence of the pig-nosed turtle (*Carettochelys insculpta*) Vocalizing Underwater. *Copeia* **105**, 29–32.

Fettiplace, R. and Fuchs, P. A. (1999). Mechanisms of hair cell tuning. *Annu Rev Physiol* **61**, 809–834.

Giles, J. C., Davis, J. A., McCauley, R. D. and Kuchling, G. (2009). Voice of the turtle: The underwater acoustic repertoire of the long-necked freshwater turtle, *Chelodina oblonga*. *J Acoust Soc Am* **126**, 434–443.

Gleich, O., Fischer, F. P., Koppl, C. and Manley, G. A. (2004). Hearing organ evolution and specialization: Archosaurs. 224–255. In *Evolution of the Vertebrate Auditory System* (eds. Manley, G. A., Popper, A. N., and Fay, R. R.) Springer New York.

Goldberg, J. M., & Brown, P. B. (1969). Response of binaural neurons of dog superior olivary complex to dichotic tonal stimuli: some physiological mechanisms of sound localization. *J Neurophysiol*, ***32*,** 613–636.

Grothe, B., Carr, C. E., Casseday, J. H., Fritzsch, B. and Koppl, C. (2004). The evolution of central pathways and their neural processing patterns. In *Evolution of the Vertebrate Auditory System* (eds. Manley, G. A., Popper, A. N., and Fay, R. R., Springer New York.

Grothe, B. and Pecka, M. (2014). The natural history of sound localization in mammals--a story of neuronal inhibition. *Front Neural Circuits* **8**, 116.

Grothe, B., Pecka, M. and McAlpine, D. (2010). Mechanisms of sound localization in mammals. *Physiol Rev* **90**, 983–1012.

Hailey, A., Rosenberg, M. E. and Pullen, A. H. (1991). An in vitro brainstem preparation preserving peripheral auditory function. *J Neurosci Meth* **39**, 217–223.

Joris, P. X., Louage, D. H., Cardoen, L., & van der Heijden, M. (2006). Correlation index: a new metric to quantify temporal coding. *Hear Res*, **216-217**, 19–30.

Kriegstein, A. R. and Connors, B. W. (1986). Cellular physiology of the turtle visual cortex: synaptic properties and intrinsic circuitry. *J Neurosci* **6**, 178–191.

Kuwada, S., Stanford, T. R. and Batra, R. (1987). Interaural phase-sensitive units in the inferior colliculus of the unanesthetized rabbit: effects of changing frequency. *J Neurophysiol* **57**, 1338–1360.

Larkum, M. E., Watanabe, S., Lasser-Ross, N., Rhodes, P. and Ross, W. N. (2008). Dendritic properties of turtle pyramidal neurons. *J Neurophysiol* **99**, 683–694.

Larsen, O. N., Christensen-Dalsgaard, J. and Jensen, K. K. (2016). Role of intracranial cavities in avian directional hearing. *Biol Cybern* **110**, 319–331.

Llinás, R. and Mühlethaler, M. (1988). Electrophysiology of guinea-pig cerebellar nuclear cells in the in vitro brain stem-cerebellar preparation. *J Physiol* **404**, 241–258.

Lu, B., Yang, W., Dai, Q. and Fu, J. (2013). Using genes as characters and a parsimony analysis to explore the phylogenetic position of turtles. *PLoS ONE* **8**, e79348.

MacLean, R. A., Harms, C. A. and Braun-McNeill, J. (2008). Propofol anesthesia in loggerhead (*Caretta caretta*) sea turtles. *J Wildlife Diseases* **44**, 143–150.

MacLeod, K. M. and Carr, C. E. (2005). Synaptic physiology in the cochlear nucleus angularis of the chick. *J Neurophysiol* **93**, 2520–2529.

Mancilla, J. G., Fowler, M. and Ulinski, P. S. (1998). Responses of regular spiking and fast spiking cells in turtle visual cortex to light flashes. *Vis Neurosci* **15**, 979–993.

Manley, G. A. (2010). An evolutionary perspective on middle ears. *Hear Res* **263**, 3–8.

Manley, G. A. (2002). Evolution of structure and function of the hearing organ of lizards. *J Neurobiol*, **53,** 202–211.

Manley, G. A. (1970). Comparative studies of auditory physiology in reptiles. *J Comp Physiol A* **67**, 363–381.

Marbey, D. and Browner, R. H. (1985). The reconnection of auditory posterior root fibers in the red-eared turtle, *Chrysemys scripta elegans*. *Hear Res* 1–4.

McAlpine, D., Jiang, D. and Palmer, A. R. (2001). A neural code for low-frequency sound localization in mammals. *Nat Neurosci* **4**, 396–401.

Miller, M. (1978). Scanning electron microscope studies of the papilla basilaris of some turtles and snakes. *Amer J Anat* **151**, 409–435.

Miller, M. R. and Kasahara, M. (1979). The cochlear nuclei of some turtles. *J Comp Neur* **185**, 221–236.

Mori, K., Nowycky, M. C. and Shepherd, G. M. (1981). Electrophysiological analysis of mitral cells in the isolated turtle olfactory bulb. *J Physiol* **314**, 281–294.

Rice, M. E. and Nicholson, C. (1990). Glutamate-and aspartate-induced extracellular potassium and calcium shifts and their relation to those of kainate, quisqualate and n-methyl-d-aspartate in the isolated turtle cerebellum. *Neurosci* **38**, 295–310.

Rodgers-Garlick, C. I., Hogg, D. W. and Buck, L. T. (2013). Oxygen-sensitive reduction in Ca2+-activated K+ channel open probability in turtle cerebrocortex. *Neurosci* **237**, 243–254.

Rutishauser, U., Kotowicz, A. and Laurent, G. (2013). A method for closed-loop presentation of sensory stimuli conditional on the internal brain-state of awake animals. *J Neurosci Meth* **215**, 139–155.

Schnee, M. E., Castellano-Munoz, M. and Ricci, A. J. (2013). Response properties from turtle auditory hair cell afferent fibers suggest spike generation is driven by synchronized release both between and within synapses. *J Neurophysiol* **110**, 204–220.

Schnee, M. E., Lawton, D. M., Furness, D. N., Benke, T. A. and Ricci, A. J. (2005). Auditory hair cell afferent fiber synapses are specialized to operate at their best frequencies. *Neuron* **47**, 243–254.

Schnee, M. E., Santos-Sacchi, J., Castellano-Muñoz, M., Kong, J.-H. and Ricci, A. J. (2011). Calcium-dependent synaptic vesicle trafficking underlies indefatigable release at the hair cell afferent fiber synapse. *Neuron* **70**, 326–338.

Shen, X. X., Liang, D., Wen, J. Z. and Zhang, P. (2011). Multiple genome alignments facilitate development of NPCL markers: A case study of tetrapod phylogeny focusing on the position of turtles. *Molec Biol Evol* **28**, 3237–3252.

Sneary, M. (1988). Auditory receptor of the red-eared turtle: II. Afferent and efferent synapses and innervation patterns. *J Comp Neurol* **276**, 588–606.

Soares, D. and Carr, C. E. (2001). The cytoarchitecture of the nucleus angularis of the barn owl (Tyto alba). *J Comp Neurol* **429**, 192–205.

Szpir, M. R., Wright, D. D., & Ryugo, D. K. (1995). Neuronal organization of the cochlear nuclei in alligator lizards: a light and electron microscopic investigation. *Journal of Comparative Neurology*, *357*(2), 217–241. http://doi.org/10.1002/cne.903570204

Valverde F. (1970) The Golgi Method. A Tool for Comparative Structural Analyses. In: Nauta W.J.H., Ebbesson S.O.E. (eds) Contemporary Research Methods in Neuroanatomy. Springer, Berlin, Heidelberg DOIhttps://doi.org/10.1007/978-3-642-85986-1_2

Viete, S., Pena, J. L. and Konishi, M. (1997). Effects of interaural intensity difference on the processing of interaural time difference in the owl's nucleus laminaris. *J Neurosci* **17**, 1815–1824.

von Hemmen, J. L., Christensen-Dalsgaard, J., Carr, C. E. and Narins, P. M. (2016). Animals and ICE: meaning, origin, and diversity. *Biol Cybern* **110**, 237–246.

Wever, E. G. and Vernon, J. A. (1956a). The sensitivity of the turtle's ear as shown by its electrical potentials. *Proc Nat Acad Sci USA* **42**, 213–220.

Wever, E. G. and Vernon, J. A. (1956b). Sound transmission in the turtle's ear. *Proc Natl Acad Sci USA* **42**, 292–299.

Wever, E. G. and Vernon, J. A. (1956c). Auditory responses in the common box turtle. *Proc Natl Acad Sci USA* **42**, 962–965.

Willis, K. L., Christensen-Dalsgaard, J. and Carr, C. E. (2013a). Auditory brain stem processing in reptiles and amphibians: roles of coupled ears. In *Insights from Comparative Hearing Research* (eds. Köppl, C., Manley, G. A., Popper, A. N., and Fay, R. R.), pp 193-225. Springer New York.

Willis, K. L., Christensen-Dalsgaard, J., Ketten, D. R. and Carr, C. E. (2013b). Middle ear cavity morphology is consistent with an aquatic origin for testudines. *PLoS ONE* **8**, e54086.

Willis, K. L., Johny, A., Carr, C. E. (2014) Tonotopic organization of the turtle brain stem. Program No. 431.09 2014 Neuroscience Meeting Planner. Washington, DC: Society for Neuroscience, 2014. Online. http://bit.ly/2vnhBHn

Wu, Y.-C. and Fettiplace, R. (1996). A developmental model for generating frequency maps in the reptilian and avian cochleas. *Biophys J* **70**, 2557–2570.

Yin, T. C. and Kuwada, S. (1983). Binaural interaction in low-frequency neurons in inferior colliculus of the cat. III. Effects of changing frequency. *J Neurophysiol* **50**, 1020–1042.

Figures

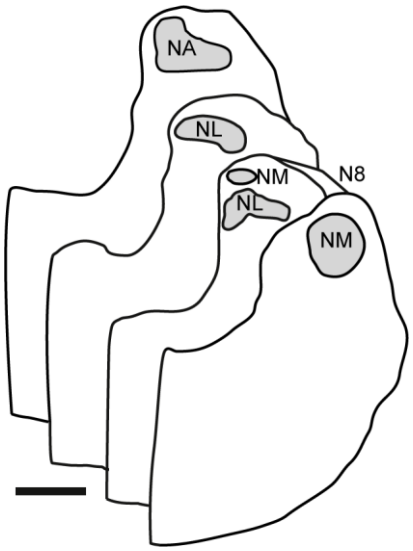

Figure 1. Rostrocaudal location of the auditory brain stem nuclei.
Schematic boundaries of the auditory nuclei in transverse section. The section containing only Nucleus Angularis (NA) is most rostral; the section containing only the Nucleus Magnocellularis (NM) is most caudal. 100 μm scale bar.

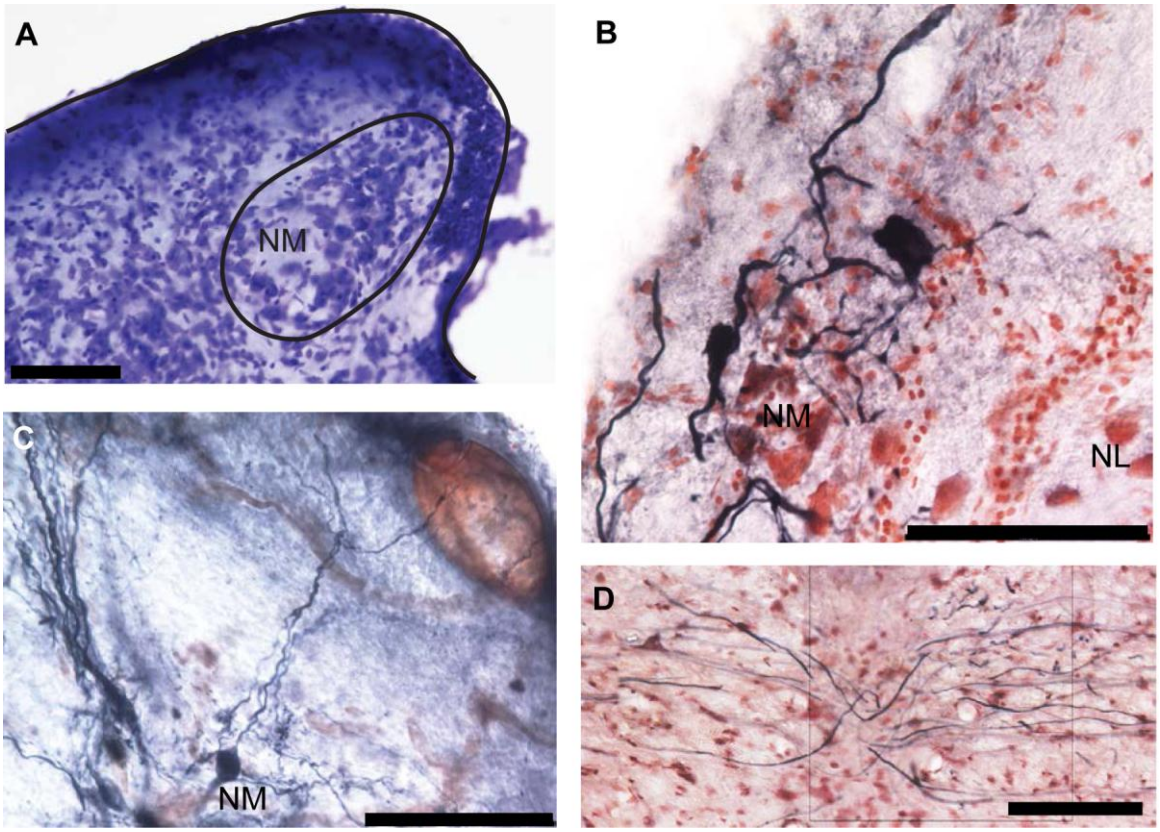

Figure 2. Nucleus Magnocellularis neurons project bilaterally to the nucleus laminaris. **A**. Cresyl violet stained transverse section of the acoustic tubercle and the nucleus magnocellularis, outlined by black line. **B**. Retrogradely labeled nucleus magnocellularis neurons in rostral nucleus magnocellularis following injection of neurobiotin in the contralateral acoustic tubercle. **C**. Retrogradely labeled nucleus magnocellularis neuron with an ascending dendrite in the VIII nerve tract. **D**. Neurobiotin labeled nucleus magnocellularis axons in the internal arcuate tract at the midline, just ventral to the fourth ventricle. All scale bars 100 μm.

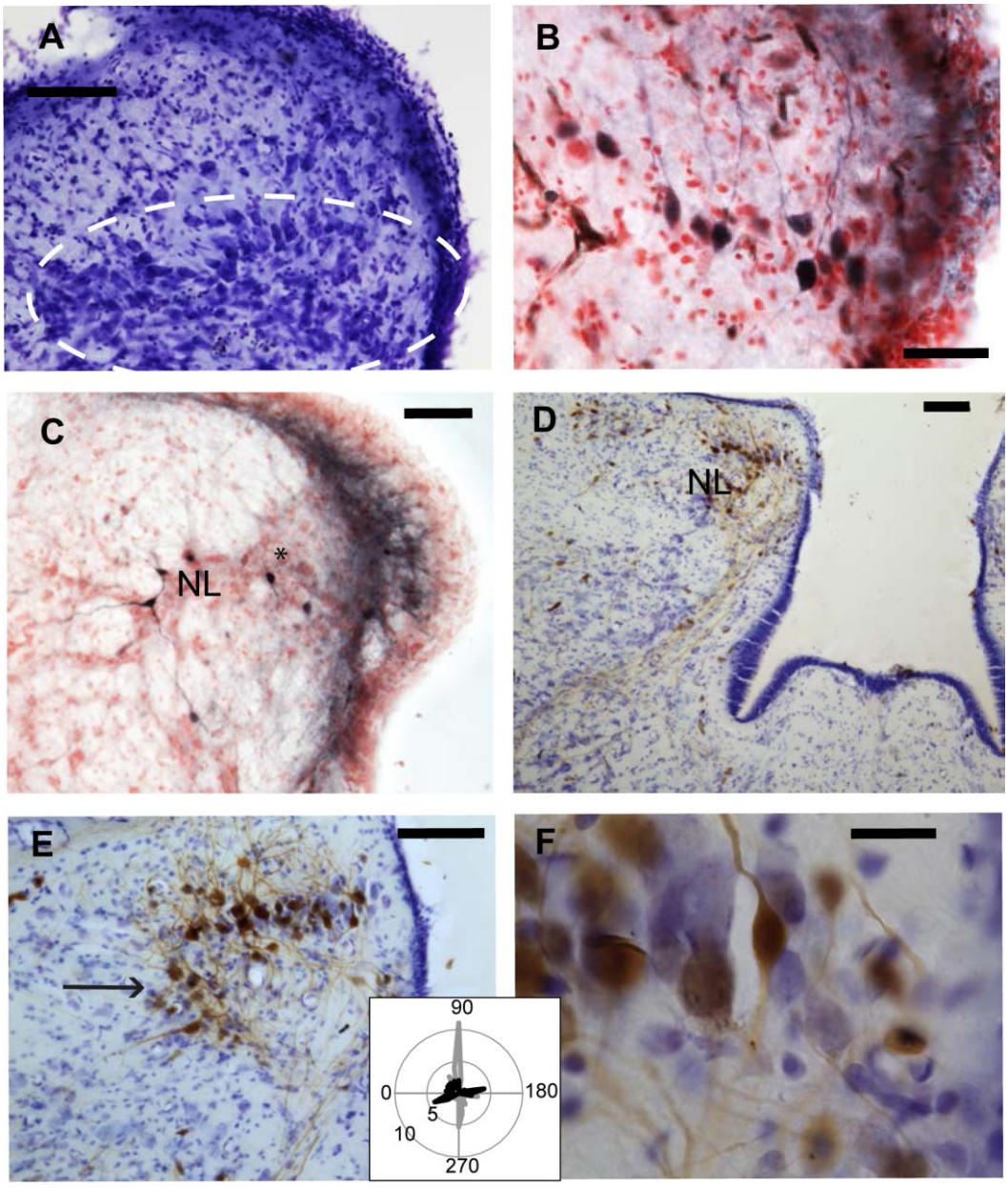

Figure 3. Nucleus Laminaris is primarily composed of vertically-oriented, bitufted neurons.

A. Cresyl violet stained transverse section through nucleus laminaris (dashed white line outlines nucleus laminaris). **B, C**. Retrogradely labeled nucleus laminaris neurons after neurobiotin injection in the torus semicircularis (TS). **D-F**. Retrogradely labeled nucleus laminaris neurons after horseradish peroxidase injection in the TS. Arrow in **E** indicates the ventral bend in lateral nucleus laminaris. **F**. Bitufted dendritic morphology in retrogradely labeled nucleus laminaris neurons magnified from **D**. 20 μm scale bar. Insert: Polar plot of dendritic orientation reveals bitufted organization in both dorsal and ventral, dendrites, n=22 neurons from the medial lamina region (grey), n=17 from the ventral bend of the lateral region of nucleus laminaris (black). Each dendrite has a value of 1 on the unit circle, with

dendritic orientation plotted with respect to the lamina of nucleus laminaris cell bodies. All scale bars 100 μm except F.

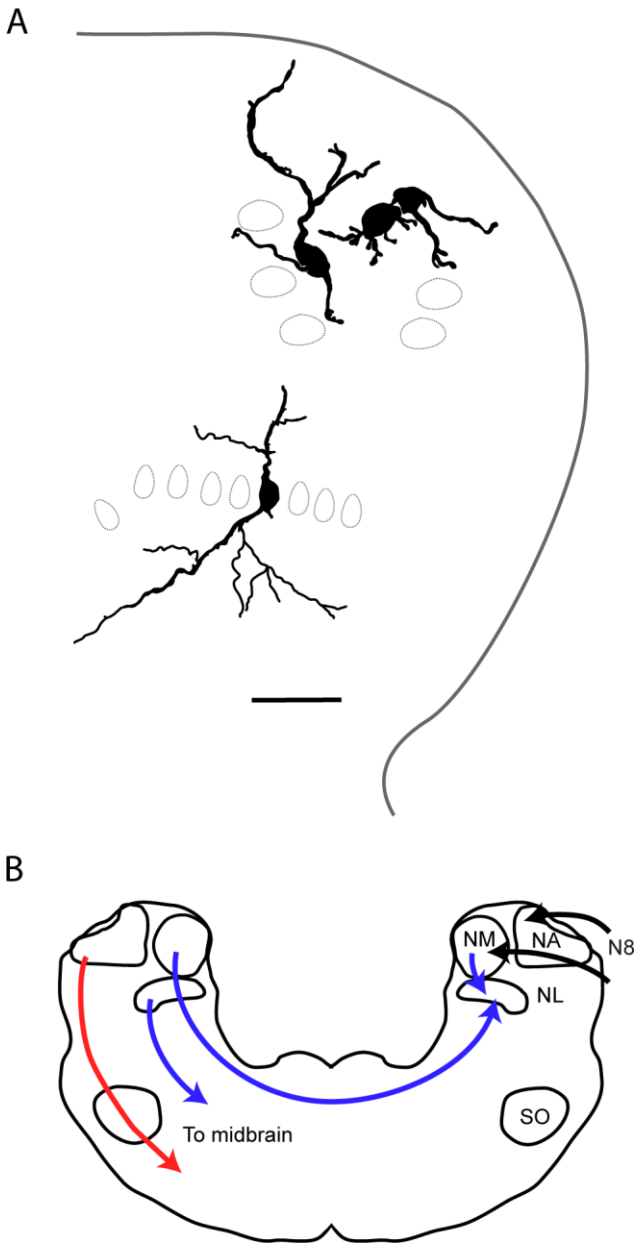

Figure 4. Summary of auditory circuits.

A. Labeled nucleus magnocellularis (above) and nucleus laminaris (below) neurons from a young turtle, drawn from a single transverse section. Rapid Golgi method (black neurons) with dotted outlines showing positions of unlabeled neurons. Grey line outlines medial acoustic tubercle. These nuclei are shown in schematic form in B. Scale = 100 µm.

B. Circuit diagram summarizing the results of tract tracing experiments. Black arrows mark the auditory nerve input to first order Nucleus Magnocellularis (NM) and Nucleus Angularis (NA). Blue arrows show the projections of the nucleus magnocellularis and nucleus laminaris (NL). The superior olive (SO) receives input from NA and NL (not shown). Red arrows show the path from nucleus angularis to the midbrain. This diagram shows the acoustic tubercle, which is defined as the portion of the brain stem that contains NA, NM, and NL

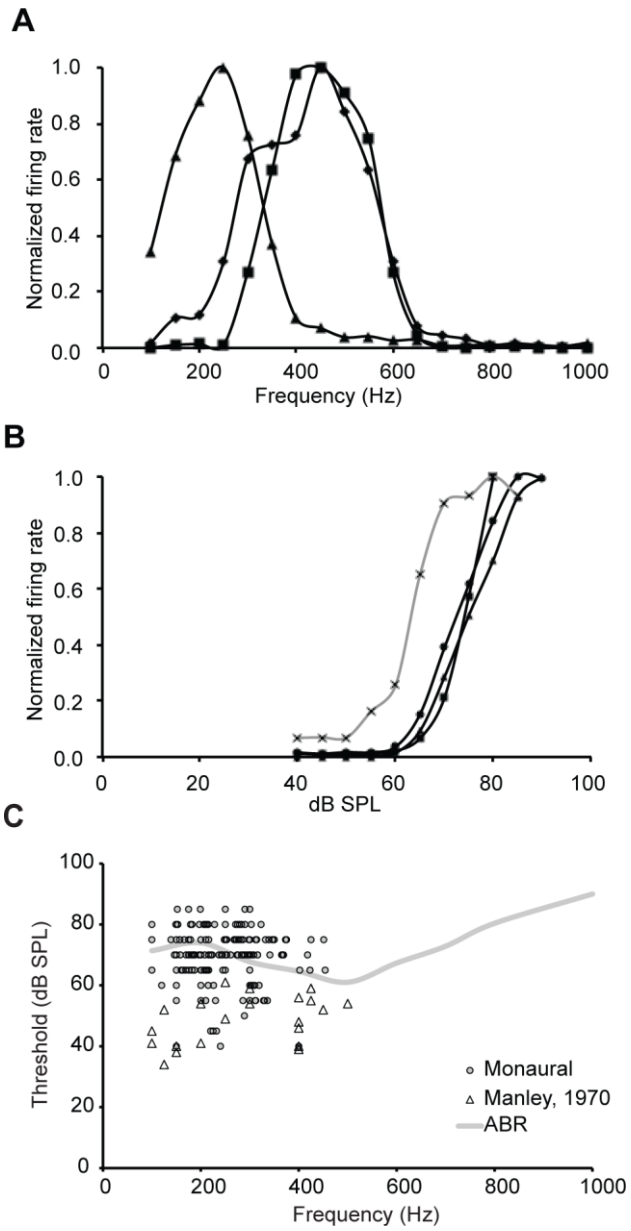

Figure 5. Physiological properties of nucleus magnocellularis neurons.

A. Representative constant intensity (80 dB) frequency–rate curves for 3 nucleus magnocellularis neurons with best frequencies between 200 and 500 Hz. **B**. Rate intensity functions of the neurons shown in A, measured at best frequency, as well as a lower threshold example (grey x, BF= 355 Hz). BFs for symbols in A and B: triangle = 226; diamond = 424, square = 475 Hz.). **C**. Threshold measured at best frequency in nucleus magnocellularis single units with ABR audiogram (Christensen-Dalsgaard et al., 2012) and in vivo cochlear nucleus data for comparison (Manley, 1970)

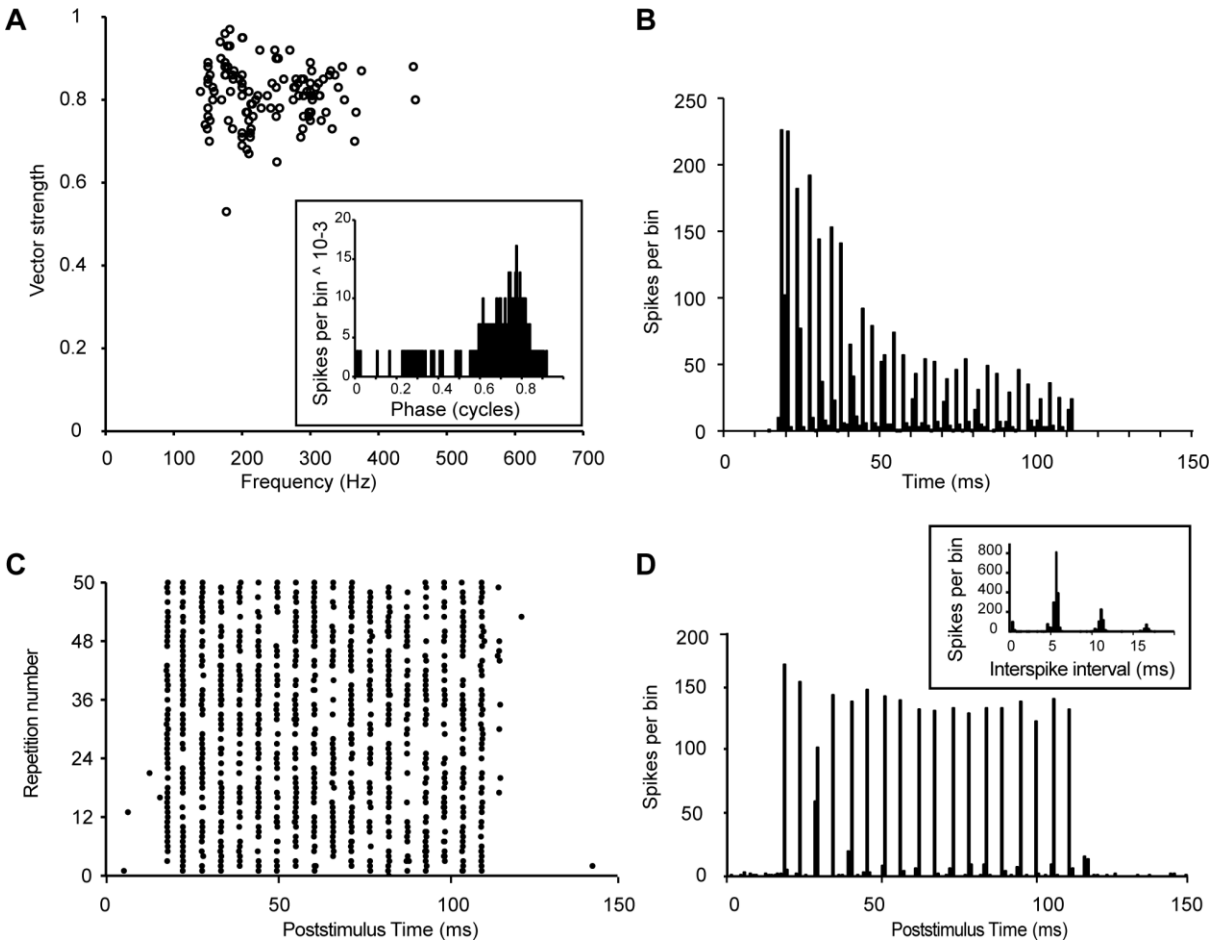

Figure 6. Phase-locking properties of nucleus magnocellularis neurons.

A. Vector strengths of single unit nucleus magnocellularis neurons. **Insert**: Example phase histogram of an nucleus magnocellularis neuron, BF=150 Hz, VS=0.88.

B. Nucleus magnocellularis PSTH with primary-like discharge pattern, BF=251 Hz.

C. Dot raster plot from 65 repetitions of stimulus to a nucleus magnocellularis neuron, BF =180 Hz, VS =0.97.

D. PSTH from the same nucleus magnocellularis neuron in as in C. Insert: Interval histogram from same unit.

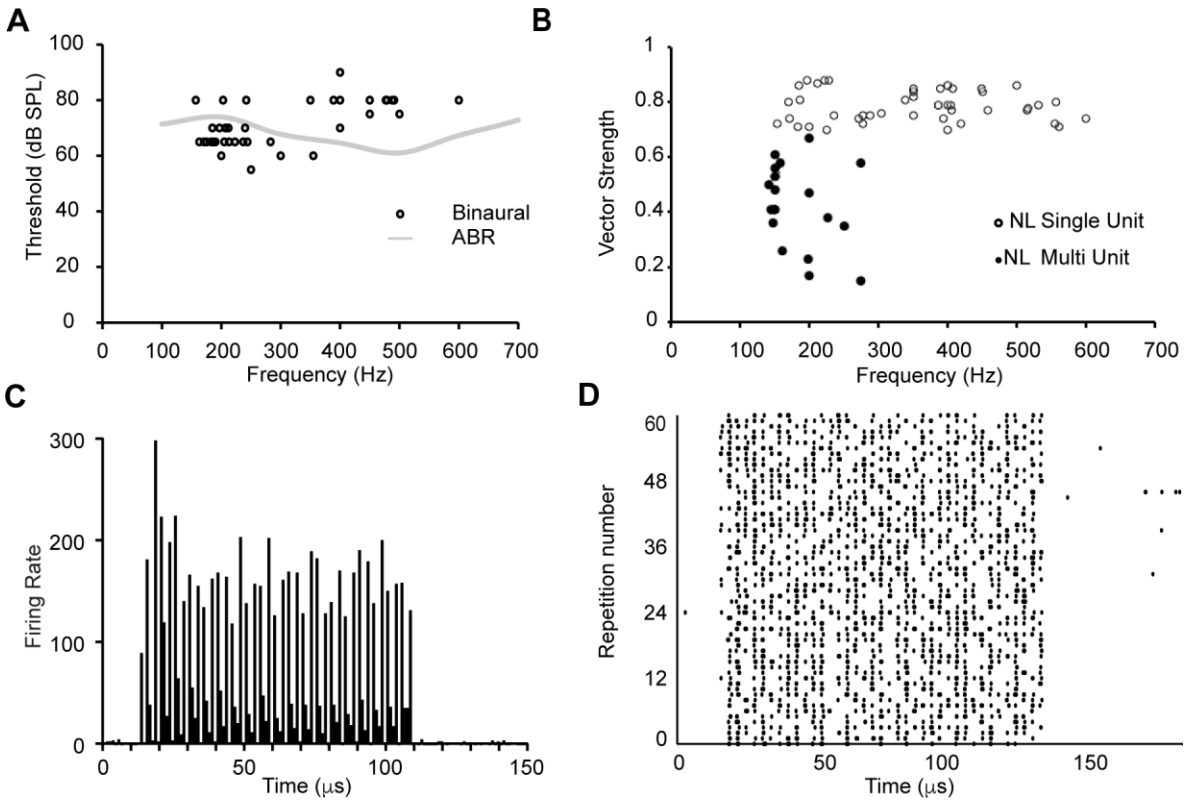

Figure 7. Physiological properties of nucleus laminaris neurons

A. Response thresholds measured at best frequency for all monaural (nucleus magnocellularis; open circles, n = 161) and binaural (nucleus laminaris; filled circles, n = 18) single units recorded.

B. Vector strengths measured at best frequency in single units (open circles) and multi-units (filled circles).

C. PSTH of a single nucleus laminaris unit at its best frequency (400 Hz).

D. Dot raster plot from 65 repetitions of the stimulus in C.

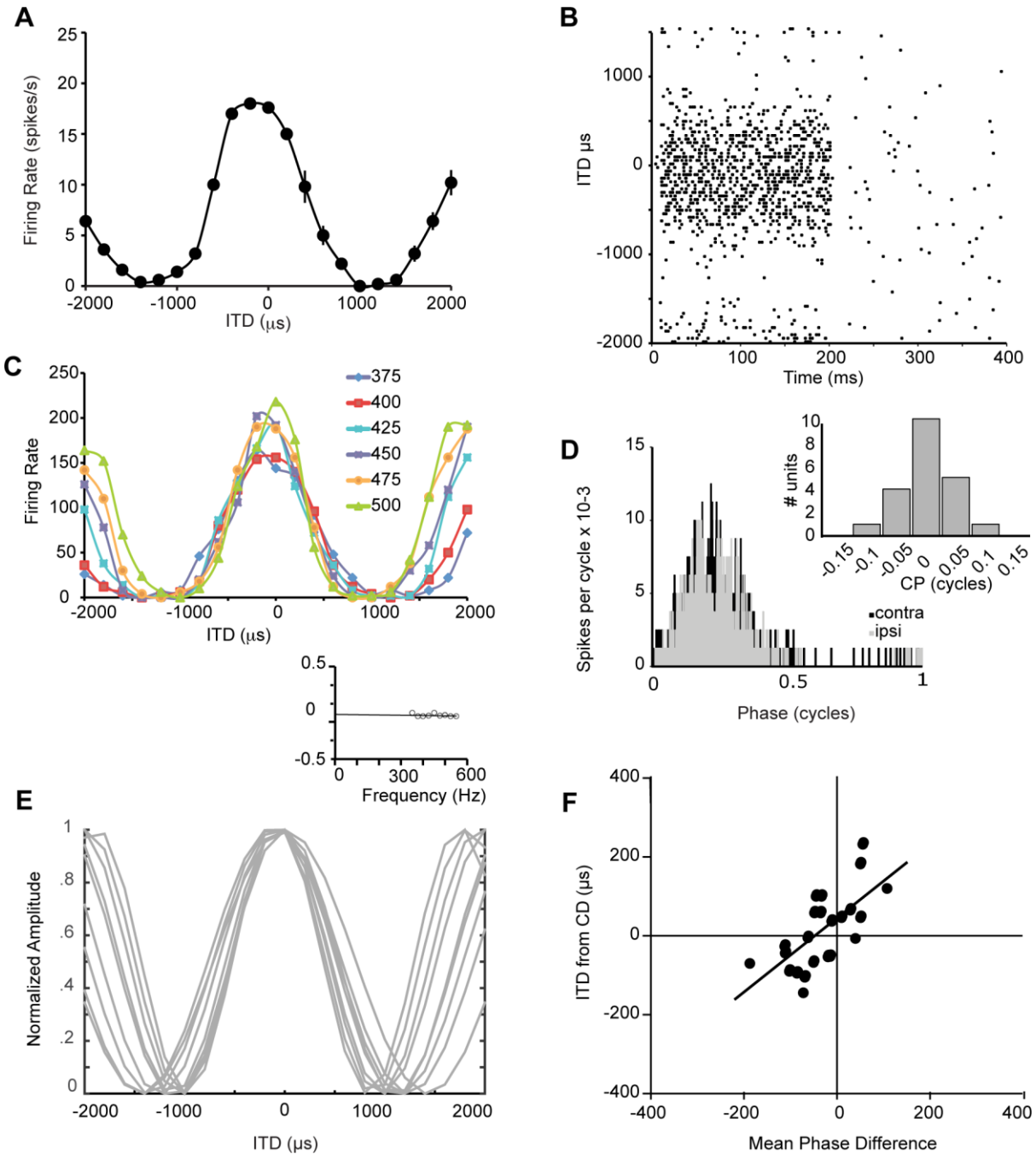

Figure 8. Turtle nucleus laminaris neurons are sensitive to ITD.

A. Response of a nucleus laminaris single unit to varying ITD at 400 Hz.

B. Raster plot from same unit.

C. ITD responses recorded in nucleus laminaris as a function of stimulus frequency (BF = 425 Hz). Interaural delay curves plot the response of this unit for a range of frequencies from 375-500 Hz. Equation for CD is $y = -0.000136x + 0.017$, $r^2 = 0.97$.

D. Period histograms of an ITD sensitive neuron in response to monaural contra- (black) and ipsilateral (gray) stimulation at 400 Hz. The difference between ipsilateral (left, black, mean phase 0.220, VS = 0.81) and contralateral (right, grey, mean phase 0.218, VS = 0.77) phase

was -5 µs, while binaural stimulation yielded a best ITD of -44µs. **Insert**: Distribution of characteristic phase for all nucleus laminaris single units yields a mean CP of -0.01 (± 0.08, n = 43), showing that the inputs to the cell at the CD are in phase.

E. Computation of characteristic delay for a single unit in left hand side nucleus laminaris, BF 450 Hz. Each curve was normalized and fit with a cosine for the 9 frequencies tested, to yield a characteristic delay (CD) of -84 µs. **Insert:** Best IPD (in cycles) determined for each of the curves shown in E, as a function of stimulation frequency (Hz). The solid line shows the linear regression. The slope of the line represents the CD, and the y-intercept, the characteristic phase (CP), $y = -0.000084x + 0.012$, $r^2 = 0.15$.

F. If laminaris neurons are excited by input from each side, and act as coincidence detectors, then differences between left and right mean phase should predict best ITD. A regression line was drawn for all data ($y = 1.0132x + 56.89$, $r^2 = 0.62$).

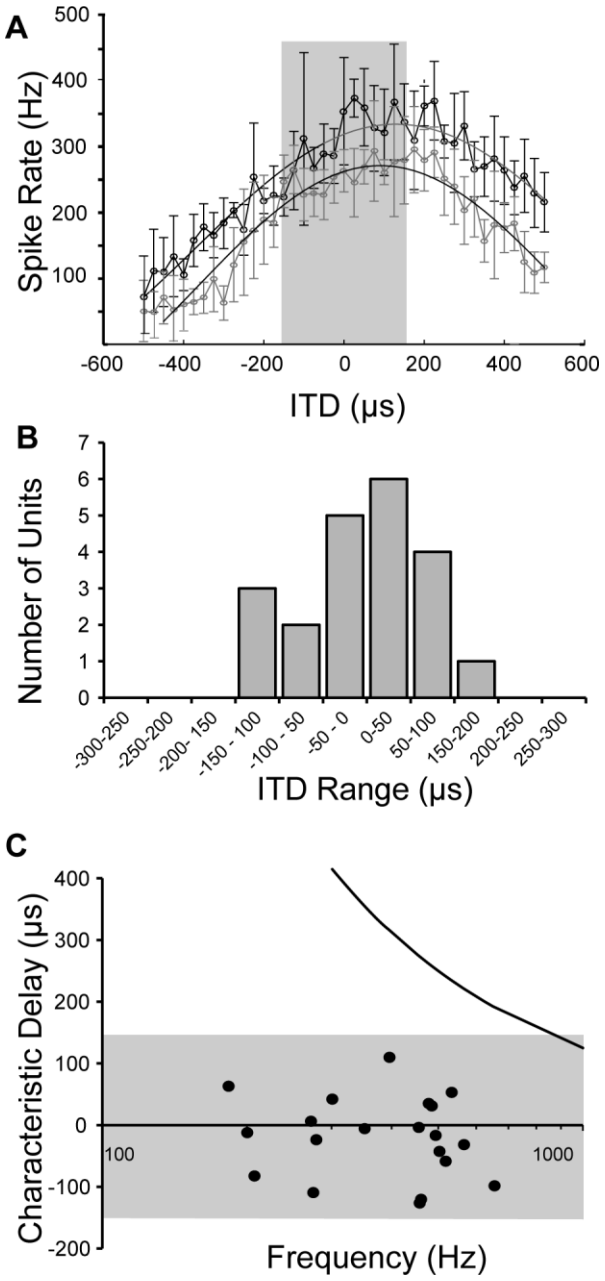

Figure 9. The majority of ITDs fall within the predicted physiological range

A. Section of a response of an nucleus laminaris single unit to varying ITD at 500 (grey curve) and 550 Hz (black curve), measured at 25 µs intervals, with 5 repetitions, ±SE, the standard error of the mean. Gray rectangle (±150 µs) designates likely physical range available to a large Red-eared Slider.

B. Distribution of all best ITDs, shown as if measured from right hand side nucleus laminaris, 50 µs bins.

C. Distribution of calculated CDs from all nucleus laminaris single units, as if measured from right hand side nucleus laminaris. Gray area (±150 µs) designates likely physical range

available to a turtle, black line shows the function (best ITD = 0.125/BF) (Grothe et al., 2010).

Table S1. Results of varying the experimental temperature and ACSF recipe.

Number of Units	Temperature (°C)	ACSF Recipe
6	18	Avian
7	18	Avian
2	18	Rodgers-Garlick, et al
2	18	Fettiplace & Crawford
8	18	Fettiplace & Crawford
6	18	Fettiplace & Crawford
0	18	Fettiplace & Crawford
1	18	Rice & Nicholson
4	18	Rice & Nicholson
0	18	Rice & Nicholson
16	20	Connors & Kriegstein
12	20	Connors & Kriegstein
7	22	Connors & Kriegstein
8	22	Connors & Kriegstein
16	22	Connors & Kriegstein
12	23	Connors & Kriegstein
30	24	Connors & Kriegstein